ARMY RESEARCH LABORATORY

Dislocation Transport in Continuum Crystal Plasticity Simulations (First-year Report)

by Richard Becker

ARL-MR-0799 **December 2011**

NOTICES

Disclaimers

The findings in this report are not to be construed as an official Department of the Army position unless so designated by other authorized documents.

Citation of manufacturer's or trade names does not constitute an official endorsement or approval of the use thereof.

Destroy this report when it is no longer needed. Do not return it to the originator.

Army Research Laboratory
Aberdeen Proving Ground, MD 21005

ARL-MR-0799 **December 2011**

Dislocation Transport in Continuum Crystal Plasticity Simulations (First-year Report)

Richard Becker
Weapons and Materials Research Directorate, ARL

REPORT DOCUMENTATION PAGE

Form Approved
OMB No. 0704-0188

1. REPORT DATE *(DD-MM-YYYY)*	2. REPORT TYPE	3. DATES COVERED (From - To)
December 2011	DRI	October 2010 to September 2011

4. TITLE AND SUBTITLE
Dislocation Transport in Continuum Crystal Plasticity Simulations (First-year Report)

5a. CONTRACT NUMBER

5b. GRANT NUMBER

5c. PROGRAM ELEMENT NUMBER

6. AUTHOR(S)
Richard Becker

5d. PROJECT NUMBER

5e. TASK NUMBER

5f. WORK UNIT NUMBER

7. PERFORMING ORGANIZATION NAME(S) AND ADDRESS(ES)
U.S. Army Research Laboratory
ATTN: RDRL-WMP-B
Aberdeen Proving Ground, MD 21005

8. PERFORMING ORGANIZATION REPORT NUMBER
ARL-MR-0799

9. SPONSORING/MONITORING AGENCY NAME(S) AND ADDRESS(ES)

10. SPONSOR/MONITOR'S ACRONYM(S)

11. SPONSOR/MONITOR'S REPORT NUMBER(S)

12. DISTRIBUTION/AVAILABILITY STATEMENT
Approved for public release; distribution unlimited.

13. SUPPLEMENTARY NOTES

14. ABSTRACT
Continuity of dislocation flux across element boundaries is introduced into a non-local, explicit finite element code using a continuum crystal plasticity constitutive model. In addition to providing enhanced coupling of the deformation field among neighboring elements, dislocation fluxes are integrated through time to give an estimate of dislocation gradients that serve as a strengthening mechanism. The results demonstrate the effects of dislocation flux continuity and the realization of a size scale associated with the gradient hardening. Numerical issues relating to spatial oscillations are identified for future work.

15. SUBJECT TERMS
Dislocation flux, crystal plasticity, gradient hardening

16. SECURITY CLASSIFICATION OF:			17. LIMITATION OF ABSTRACT	18. NUMBER OF PAGES	19a. NAME OF RESPONSIBLE PERSON
a. REPORT	b. ABSTRACT	c. THIS PAGE			Richard Becker
Unclassified	Unclassified	Unclassified	UU	32	19b. TELEPHONE NUMBER (*Include area code*) (410) 278-7980

Contents

List of Figures

Acknowledgment

The author is grateful for the support of this work through the Director's Research Initiative at the U.S. Army Research Laboratory.

INTENTIONALLY LEFT BLANK.

1. Introduction

Traditional metal plasticity models, formulated in terms of strain rates and stresses and incorporated in large-scale numerical analyses, provide useful solutions for a wide range of problems. Details of the material microstructure interactions that govern the deformation response are assumed to occur at length scales not resolvable by the simulations and are captured implicitly in the constitutive relations. For example, dependence of the yield strength on grain size through the Hall-Petch effect can be incorporated by including grain size in the constitutive model without tracking the details of dislocation interactions with grain boundaries.

In simulations with resolution at the grain scale, as in multiscale modeling, the length scales dictating some hardening mechanisms are comparable to the numerical discretization. The torsion experiments of Fleck and Hutchinson (1997) clearly demonstrate increased strength with decreasing size for wires 10's of microns in diameter. The strengthening is attributed to gradients in the crystal lattice orientation, which create boundaries where dislocations accumulate. These structures both store energy and provide resistance to further dislocation motion (e.g., Baskaran et al., 2010). Applying traditional crystal plasticity models (e.g., Asaro, 1983; Peirce et al., 1983) to investigate the strengthening in a multiscale framework will not be successful because the models are formulated in terms of traditional continuum variables of strain rate and stress, and there is no underlying microstructure length scale that would produce a size effect.

Numerous studies over the past decade have investigated ways to incorporate a length scale into the continuum crystal plasticity model. Most focus on microstructure gradients, as it is recognized that both the Hall-Petch effect and the results of Fleck and Hutchinson are tied to gradients. To cite just a few of the many examples, models have examined continuously distributed dislocations (Acharya, 2001), dislocation density gradients (Arsenlis et al., 2004), and gradient related state variables (Gurtin et al., 2007; Gerken and Dawson, 2008; Mayeur et al., 2011). These formulations all introduce additional variables into the solution, which creates two difficulties. The first is fitting these into a solution scheme with appropriate evolution equations, and the second is determining an appropriate prescription for boundary conditions on the new variables. The former is typically the focus of the research. The latter often remains an open issue. For example, what is the value of a strain gradient at a free surface versus an interface, or how should dislocation density be prescribed as a boundary condition?

When using the traditional crystal plasticity model in a finite element code, the deformation of neighboring elements is only connected through shared nodal displacements and force equilibrium at the nodes. Even though dislocations associated with slip travel through the material, the transmission of dislocations from one element to another is not represented, and the resulting coordination in slip deformation is not captured. The effective result is that all finite element boundaries are infinite sources and sinks for dislocations. Advanced crystal plasticity

formulations, such as those based on lattice orientation gradients, often include the continuity of dislocation flux across finite element boundaries as a byproduct. However, the importance of this physical constraint is not explored independently.

The goal of the current work is to determine if a simpler approach can be used to address the length scale and other deficiencies of the classical crystal plasticity model. It is a search in pursuit of Occam's razor, the law of parsimony. The starting point is enforcing dislocation flux continuity across finite element boundaries. This uses existing solution variables and the boundary conditions are conceptually straightforward. Dislocation flux is unconstrained at free surfaces and zero at rigid boundaries and intermediate at grain boundaries that are sources and sinks for dislocations. The flux gradients can be used to infer the evolution of dislocation gradients that lead to lattice orientation gradients.

This report presents the formulation and results from the first year's effort on the two-year Director's Research Initiative (DRI) project. The finite element code, the crystal plasticity model, and the dislocation flux continuity relations are presented in section 2. Section 3 contains results from verification calculations and initial simulations exploring the effects of flux continuity and hardening associated with slip gradients. The report concludes with a discussion of the results and several issues that were identified.

2. Finite Element Code, Crystal Plasticity Model, and Slip Continuity

The proposed model is non-local, where the material response in a finite element depends directly on the structure evolution in neighboring elements. Only a few existing finite element frameworks would accommodate such a model without substantial modifications. Another goal, that further restricts the use of existing software, is an explicit dynamic implementation that can be used in high rate deformation applications. Given the requirements, it was determined that it would be more efficient and more effective to create a simple, explicit finite element research code rather than to modify an existing code and its data structures. The finite element model is described in section 2.1.

Modules for the underlying crystal plasticity model are taken from an existing implementation in ALE3D (Becker, 2004). A brief description is given below. An idealized, two-dimensional (2-D) crystal geometry with three slip systems, oriented 60° apart, was implemented so that the formulation and algorithm development could be carried out more efficiently. Time integration of the constitutive model within the finite element code departs significantly from standard finite element time integration schemes and is described in section 2.4.

2.1 Explicit Finite Element Framework

A 2-D, explicit finite element code was created as a framework to develop and evaluate the slip continuity model. It uses either constant strain triangle elements in a crossed-triangle configuration (Nagtegaal, Parks, and Rice, 1974) or constant strain quadrilaterals with hourglass control (Flanagan and Belytschko, 1981). Time integration is with the second-order accurate "leap-frog" method, where positions, forces, and accelerations are evaluated at full time step intervals and velocities are evaluated at the midpoints of the time steps. In the absence of body forces, the momentum equation determines accelerations by

$$\ddot{\boldsymbol{x}}_t = (\boldsymbol{\nabla} \cdot \boldsymbol{\sigma})/\rho_t \,. \tag{1}$$

Updates to the velocity and position are evaluated, respectively, as

$$\dot{\boldsymbol{x}}_{t+\Delta t/2} = \dot{\boldsymbol{x}}_{t-\Delta t/2} + \ddot{\boldsymbol{x}}_t \Delta t \tag{2}$$

and

$$\boldsymbol{x}_{t+\Delta t} = \boldsymbol{x}_t + \dot{\boldsymbol{x}}_{t+\Delta t/2} \Delta t \,. \tag{3}$$

Written in the discretized finite element context, equation 1 becomes

$$\ddot{\boldsymbol{x}}_t^J = \left(-\sum_M \boldsymbol{\sigma}^M \cdot \boldsymbol{B}^{JM} V^M \right) / m^J \,, \tag{4}$$

where $\boldsymbol{B}^{JM}$ is the derivative of the finite element shape function for node J of element M, m^J is the node mass, and V^M is the element volume. The summation is over all of the elements surrounding the node. Equation 4 implies a lumped mass matrix. The nodal mass contribution from each element is determined from integration of the element volume rather than simply dividing the element mass by four. This properly accounts for the element shape and provides a more consistent mass for the Flanagan-Belytschko element.

The velocity gradient for element M is calculated using the mid-step configuration when determining $\boldsymbol{B}^{JM}$ in order to achieve second-order accurate strain integration,

$$\boldsymbol{L}^M = \sum_J \dot{\boldsymbol{x}}^J \otimes \boldsymbol{B}^{JM} \,. \tag{5}$$

2.2 Crystal Kinematics

The crystal plasticity model used in the current study follows from the widely used kinematic framework described by Asaro (1983) and first implemented in a finite element framework by Peirce, Asaro, and Needleman (1983). The deformation gradient, $\boldsymbol{F}$, is notionally decomposed into elastic and plastic parts, $\boldsymbol{F^e}$ and $\boldsymbol{F^p}$, respectively

$$\boldsymbol{F} = \boldsymbol{F}^e \cdot \boldsymbol{F}^p \tag{6}$$

The elastic part accounts for distortion and rotation of the crystal lattice, and the plastic part represents slip on predefined crystal planes and directions that moves material but does not alter the underlying crystal lattice. This is shown schematically in figure 1. The plastic part can be envisioned as the accumulated effect of slip on each slip system, γ^{α}, with the reference crystallographic plane normals given by $\boldsymbol{m}_0^{\alpha}$ and reference slip directions denoted by $\boldsymbol{s}_0^{\alpha}$.

$$\boldsymbol{F}^{p} = \sum_{\alpha=1}^{N_{sys}} \gamma^{\alpha}\, \boldsymbol{s}_0^{\alpha} \otimes \boldsymbol{m}_0^{\alpha} + \boldsymbol{I} \tag{7}$$

The elastic part of the deformation gradient orients the lattice in the current configuration and distorts it consistent with the applied stresses.

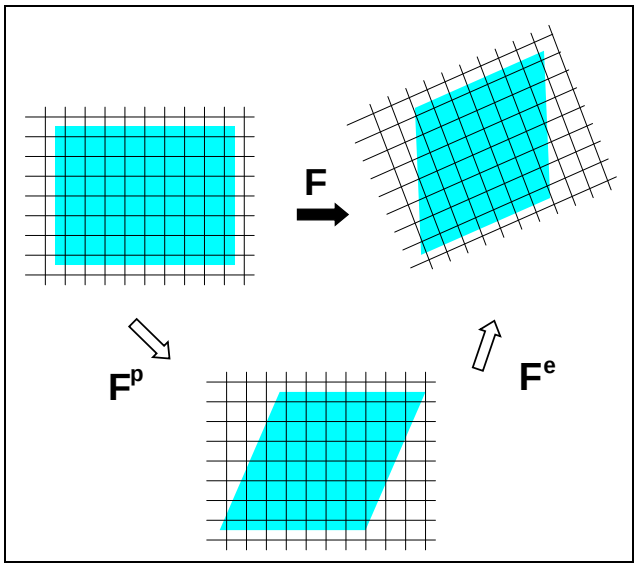

Figure 1. Representation of the elastic-plastic decomposition of the deformation gradient.

The intermediate configuration illustrated in figure 1 does not really exist, but it serves as a convenient reference frame for constructing the slip model. It is important to note that, while deformation gradient describes a compatible deformation field with no holes and a smoothly varying displacement field, the notional deformation fields associated with the elastic and plastic parts do not. A crystal subjected to a non-affine (inhomogeneous) deformation, and conceptually unloaded elastically to the intermediate configuration shown in figure 1, may have cracks, holes, and/or overlaps. In addition, the total slip form represented in equation 7 and figure 1 is only applicable for small deformations or if the relative slip rates on the various slip systems are constant over the deformation history. The rate form of the model is more general.

The velocity gradient, $\boldsymbol{L}$, resulting from this kinematic description, creates an additive decomposition into elastic and plastic parts:

$$\boldsymbol{L} = \dot{\boldsymbol{F}} \cdot \boldsymbol{F}^{-1} = \dot{\boldsymbol{F}}^{e} \cdot \boldsymbol{F}^{e^{-1}} + \boldsymbol{F}^{e} \cdot \dot{\boldsymbol{F}}^{p} \cdot \boldsymbol{F}^{p^{-1}} \cdot \boldsymbol{F}^{e^{-1}} \overset{\text{def}}{=} \boldsymbol{L}^{e} + \boldsymbol{L}^{p} \tag{8}$$

Applying the elastic part of the velocity gradient indicated by equation 8 to the rate form of equation 7 gives the plastic part of the velocity gradient as

$$\boldsymbol{L}^p = \sum_{\alpha=1}^{N_{sys}} \dot{\gamma}^\alpha \left(\boldsymbol{F}^e \cdot \boldsymbol{s}_0^\alpha \otimes \boldsymbol{m}_0^\alpha \cdot \boldsymbol{F}^{e^{-1}} \right) = \sum_{\alpha=1}^{N_{sys}} \dot{\gamma}^\alpha \, \boldsymbol{s}^\alpha \otimes \boldsymbol{m}^\alpha , \tag{9}$$

where $\boldsymbol{s}^\alpha$ and $\boldsymbol{m}^\alpha$ are, respectively, the slip direction and slip plane normal in the current configuration. The symmetric part of $\boldsymbol{L}^p$ is the plastic part of the rate of deformation tensor and the anti-symmetric part is the plastic spin, defined respectively by

$$\boldsymbol{d}^p = \frac{1}{2} \sum_{\alpha=1}^{N_{sys}} \dot{\gamma}^\alpha \, (\boldsymbol{s}^\alpha \otimes \boldsymbol{m}^\alpha + \boldsymbol{m}^\alpha \otimes \boldsymbol{s}^\alpha) = \sum_{\alpha=1}^{N_{sys}} \dot{\gamma}^\alpha \, \boldsymbol{P}^\alpha \quad \text{and} \tag{10}$$

$$\boldsymbol{w}^p = \frac{1}{2} \sum_{\alpha=1}^{N_{sys}} \dot{\gamma}^\alpha \, (\boldsymbol{s}^\alpha \otimes \boldsymbol{m}^\alpha - \boldsymbol{m}^\alpha \otimes \boldsymbol{s}^\alpha) \, . \tag{11}$$

2.3 Crystal Slip Constitutive Relations

The crystal slip constitutive model relates the loading on the slip systems to the slip rate. A traditional approached is used, and the model is similar to that employed by Peirce, Asaro, and Needleman (1983). The loading variable, τ^α, is constructed to be work conjugate to the slip rate so that the plastic dissipation on the slip systems is equal to the plastic dissipation expressed in terms of the continuum variables:

$$\boldsymbol{\sigma} : \boldsymbol{d}^p = \sum_{\alpha=1}^{N_{sys}} \dot{\gamma}^\alpha \, [\, \boldsymbol{\sigma} : \boldsymbol{P}^\alpha] = \sum_{\alpha=1}^{N_{sys}} \dot{\gamma}^\alpha \, \tau^\alpha \ , \tag{12}$$

where $\boldsymbol{P}^\alpha$ is defined in equation 10.

The resolved shear stress, τ^α, provides loading on the slip system, which results in a slip rate. A simple power law rate model is used here

$$\dot{\gamma}^\alpha = \dot{\gamma}_0^\alpha \left(\left| \frac{\tau^\alpha}{g^\alpha} \right| \right)^{1/m} sign(\tau^\alpha) \ . \tag{13}$$

The strength of the slip system, g^α, is typically a function of the deformation, and a simple power law form is assumed,

$$g^\alpha = g_0^\alpha (1 + \beta \, \gamma)^n \, , \tag{14}$$

where γ is the accumulated slip,

$$\gamma = \int_0^t \left[\sum_{\alpha=1}^{N_{sys}} |\dot{\gamma}^\alpha| \right] dt \ . \tag{15}$$

In all of the simulations, $g_0^\alpha = 33$ MPa, $n = 0.2$, $\dot{\gamma}_0^\alpha = 1$ s^{-1}, $m = 0.002$, and $\rho_0 = 2.7$ g/cm^3. For the simulations with strain hardening in section 3.3, $\beta = 20$. For the simulations in sections 3.1 and 3.2, the strength is assumed to be constant by setting $\beta = 0$. This facilitates focus on the new aspects of the model without the difficulty of deconvolving slip continuity effects from strain hardening effects.

A complete anisotropic elastic treatment is available (Becker, 2004). However, as with strain hardening, inclusion of anisotropic elastic effects may create ambiguities when attributing behaviors to the new model features. Consequently, the elastic constants used in all simulations create an isotropic elastic response. The shear modulus is taken to be 27 GPa and the bulk modulus is 58 GPa.

2.4 Non-local Slip Modeling

The introduction slip continuity between neighboring finite elements is the main focus of this work. With the traditional crystal plasticity model and the finite element formulations described previously, the deformation of neighboring elements is only connected through shared nodal displacements and force equilibrium at the nodes. Even though dislocations associated with slip travel through the material, the transmission of dislocations from one element to another is not represented, and the resulting coordination in slip deformation is not captured. The effective result is that all finite element boundaries are infinite sources and sinks for dislocations. When viewed in terms of the elastically unloaded, intermediate configuration described in section 2.2, all of the discontinuity associated with the intermediate configuration is located at the element boundaries. Gradients of lattice orientation within elements are not captured when constant strain elements are used.

The goal is to create the simplest model possible that captures the mutual effect of slip continuity on neighboring elements. This is conceptually most straightforward for edge dislocations in an idealized 2-D geometry where the directions of dislocation motion and slip are coincident. Screw dislocations, in which the material motion is orthogonal to the dislocation motion, do not exist in the 2-D crystal representation. These would create shear out of the plane.

2.4.1 Slip Continuity

The simplest approach is to enforce continuity of slip without changing anything else in the crystal plasticity formulation. The basic picture is that edge dislocations move along the slip direction from one element to another. The flux of dislocations crossing an area (one in-plane dimension and the out-of-plane dimension, *w*, assumed to be unity) for each slip system is

$$\dot{\phi} = \rho_{dis}^\alpha \, v^\alpha \boldsymbol{s}^\alpha \cdot \boldsymbol{n} \, , \tag{16}$$

where ρ_{dis}^{α} is the dislocation density (number of dislocations per unit in-plane area), v^{α} is the dislocation velocity, and $\boldsymbol{n}$ is the outward normal to the element face. Continuity is enforced by requiring that the flux exiting one element through a face equal the flux entering the neighboring element through the same face. The dislocation density, velocity, and the Burgers vector, *b* (displacement caused by the passing of a dislocation), are related to shearing rate by Orowan's equation:

$$\dot{\gamma}^{\alpha} = \rho_{dis}^{\alpha}\, v^{\alpha}\, b. \tag{17}$$

For a shared element face, and assuming that the Burgers vector is constant, the flux continuity in the idealized 2-D crystal can be represented as

$$(\dot{\gamma}^{\alpha}\boldsymbol{s}^{\alpha})_{e1} \cdot \boldsymbol{n} = (\dot{\gamma}^{\alpha}\boldsymbol{s}^{\alpha})_{e2} \cdot \boldsymbol{n}\ , \tag{18}$$

where subscripts *e1* and *e2* denote the two elements sharing a face and $\boldsymbol{n} = \boldsymbol{n}_{e1} = -\boldsymbol{n}_{e2}$. The slip rates and slip direction are generally different for two adjacent elements in an inhomogeneous deformation field. The constraint can be enforced naturally if the primary flux variable for the solution were associated with the element faces. This approach is pursued.

In an implicit formulation, this type of constraint would be enforced through the global system of equations. Such a global system solution is impracticable in an explicit dynamic approach where many time steps are required to track the wave motion.

Here, an operator split approach is applied, where dislocation fluxes are determined on element faces during a first phase, and the deformation due to those fluxes is applied in the subsequent phase. This is facilitated by creating a two-pass material model. The first pass is the standard crystal plasticity model, outlined in sections 2.2 and 2.3, except that the only results retained from the model are the slip rates. The stresses and updates to the history variables are discarded. The slip rates from this first phase are averaged on the faces, giving values denoted as $\dot{\gamma}^{\alpha f}$, where the superscript f refers to the face number associated with the element.

The slip rate for the element (either three-node triangle or four-node quadrilateral) is then determined from average dislocation flux through the faces as

$$\dot{\gamma}^{\alpha} = \sum_{f=1}^{3\ or\ 4} \left(\dot{\gamma}^{\alpha f} \left|\boldsymbol{s}^{\alpha} \cdot \boldsymbol{n}^{f}\right| l^{f}\right) \Big/ \sum_{f=1}^{3\ or\ 4} \left(\left|\boldsymbol{s}^{\alpha} \cdot \boldsymbol{n}^{f}\right| l^{f}\right). \tag{19}$$

where l^{f} is the length of the element face. This resulting element-centered slip rate is then used directly in a modified crystal plasticity module to update the stress and history variables for the next time step.

Free surfaces, where dislocations exit without constraint, are treated as natural boundary conditions by this approach. No special boundary conditions need to be applied for free surfaces. Stiff boundaries, such as elastic substrates or hard precipitates, and tightly bound second phases,

can be modeled by zeroing the slip rate at those interfaces. Surfaces with intermediate constraint that may allow the passage, generation, or absorption of some dislocations, such as weak precipitates or grain boundaries, could be simulated by reducing the slip commensurate with the resistance of the boundary. Ideally, Robertson's rules (Lee et al., 1989) for transmission of dislocations across grain boundaries could be implemented.

2.4.2 Slip Gradient Effects

A finite element in a Lagrangian crystal plasticity simulation represents a fixed material volume with dislocations fluxing into and out of the volume and dislocation generation within the volume. With the slip rates on faces used as primary solution variables, a straightforward application of Reynolds transport theorem over the volume *V* and enclosing surface *S*,

$$\frac{d}{dt}\int_V \rho_{dis}^{\alpha}\, dV = \int_V \frac{\partial \rho_{dis}^{\alpha}}{\partial t} dV + \int_S \rho_{dis}^{\alpha}\, v^{\alpha} \boldsymbol{s}^{\alpha} \cdot \boldsymbol{n}\, dS\,, \tag{20}$$

can be used, along with dislocation nucleation and annihilation rates, to estimate a lower bound on the population of statistically stored dislocations in an element volume. The first term on the right-hand side represents generation of dislocations within an element and the second term represents accumulation due to flux across the element boundaries. Applying the divergence theorem, and recognizing that the slip direction is constant throughout the element volume for the chosen element types, the last term can be manipulated as

$$\int_S \rho_{dis}^{\alpha}\, v^{\alpha} \boldsymbol{s}^{\alpha} \cdot \boldsymbol{n}\, dS = \int_V \boldsymbol{\nabla} \cdot (\rho_{dis}^{\alpha}\, v^{\alpha} \boldsymbol{s}^{\alpha})\, dV = \int_V \boldsymbol{s}^{\alpha} \cdot \boldsymbol{\nabla}(\rho_{dis}^{\alpha}\, v^{\alpha})\, dV = \int_V b^{-1} \boldsymbol{s}^{\alpha} \cdot \boldsymbol{\nabla} \dot{\gamma}^{\alpha}\, dV \tag{21}$$

The third integrand of equation 21 indicates the gradient in dislocation flux projected along the slip direction, and the last integrand relates the dislocation flux gradient to the gradient in slip rate through Orowan's equation. The flux can be evaluated directly from the surface integral as

$$\int_S \rho_{dis}^{\alpha}\, v^{\alpha} \boldsymbol{s}^{\alpha} \cdot \boldsymbol{n}\, dS = \sum_{f=1}^{3\ or\ 4} \rho_{dis}^{\alpha}\, v^{\alpha} \boldsymbol{s}^{\alpha} \cdot \boldsymbol{n}^{f}\, l^{f} w = \sum_{f=1}^{3\ or\ 4} \dot{\gamma}^{\alpha f} \boldsymbol{s}^{\alpha} \cdot \boldsymbol{n}^{f}\, l^{f}\, b^{-1} w\,, \tag{22}$$

where *w* is the out-of-plane depth. Taken together, equations 21 and 22 give the gradient of dislocation flux along a slip plane in terms of the associated slip rates on the element faces.

The dislocations stored within an element volume are associated with an imbalance of dislocations entering and leaving the element, which is related to the dislocation flux gradients of equation 21. If occurring on a single slip plane, these dislocations create pileups leading to the Hall-Petch relation. If the excess dislocations are on many parallel slip planes, they are often associated with geometrically necessary dislocations accommodating the crystal lattice misorientation between subgrains. These subgrain walls serve as barriers to dislocation motion,

so both scenarios are hardening mechanisms. The potency of these mechanisms is related to the number of dislocations over a distance, and this provides a material length scale. Many of the extensions to the crystal plasticity model are based on pile-ups and geometrically necessary dislocations with the intent of incorporating a size scale into the model.

As indicated earlier, the stored dislocations result from the dislocation flux gradients integrated through time. Using Orowan's relation, the dislocation flux gradients are related to slip rate gradients, as shown in equation 21. In the current treatment, the content of stored dislocations is estimated by assuming a simple time integration of the slip rates from equations 21 and 22:

$$\frac{1}{V}\int_t\left\{\int_V \boldsymbol{s}^\alpha\cdot\boldsymbol{\nabla}\dot{\gamma}^\alpha\,dV\right\}dt \simeq \frac{1}{V}\int_V \boldsymbol{s}^\alpha\cdot\boldsymbol{\nabla}\gamma^\alpha\,dV = \frac{1}{V}\sum_{f=1}^{3\ or\ 4}\gamma^{\alpha f}\boldsymbol{s}^\alpha\cdot\boldsymbol{n}^f\,l^f w \ \stackrel{\text{def}}{=}\ \nabla\gamma^\alpha. \qquad (23)$$

The time integration is only approximate because the path dependent aspects of the solution are neglected in this approach. $\nabla\gamma^\alpha$ is a scalar measure, with units of inverse length, of the accumulated slip gradient projected along the slip plane. It serves as a surrogate for the dislocation content, either pipe-ups or geometrically necessary dislocations.

The slip gradient is multiplied by the shear modulus, μ, and a fixed material length scale factor, λ, as a modification to the slip system strength given in equation 14:

$$g^\alpha = g_0^\alpha\left(1 + a\mu\lambda\sum_{\alpha=1}^{N_{sys}}\nabla\gamma^\alpha\right)(1+\beta\,\gamma)^n\,. \qquad (24)$$

The parameter a governs the strength of the gradient contribution. For the simulations where gradient effects are included, $a\lambda = 0.001$ μm, and $a = 0.0$ for the simulations where the slip gradient does not affect the hardening.

3. Results

The primary result from the fiscal year 2011 (FY11) effort on this DRI is the non-local, explicit finite element code running a modified, operator-split, crystal plasticity model, where dislocation flux continuity is enforced through common variables at element boundaries and the crystal flow strength is modified based on calculated slip gradients. The code has restart capability and writes plot files in XDMF format (XDMF, 2011) for viewing with a standard finite element post-processor. Since the focus of the work is introducing physics into the crystal plasticity model, large parallel runs are not needed and the implementation is serial.

3.1 Verification of Flux Continuity Implementation

The finite element framework, the crystal model, and the gradient calculations have been verified through numerous unit program tests and large-scale simulations with known solutions and behaviors. The finite element and crystal model were checked with standard evaluations, which are not presented here. An example of a flux gradient verification simulation is the simple shear deformation shown in figures 2–4. Here the non-hardening single crystal sample is 10 μm tall and 5 μm wide with an element size of 0.5 μm. The top surface is given a constant velocity of 10^5 μm/μs to the left and the bottom 3 μm of the crystal is held fixed. The intent is to provide an abrupt transition from no deformation in the lower one-third of the crystal to a simple shear deformation in the upper two-thirds. Periodic boundary conditions are applied across the 5-μm direction, so the multiple elements in the *x*-direction serve only to verify that the periodic boundary conditions are applied properly.

Figure 2 shows slip rates and the gradient of the slip rates for slip systems 1 and 3 when the lattice is initially rotated 15° from the reference orientation. Slip continuity is not enforced in this simulation, and it provides a baseline result using the traditional crystal plasticity model. Focusing on slip system 1, the slip rates are 0.007829 μs^{-1} in the sheared region and zero in the non-sheared region below it (figure 2a). The slip rate at the interface between the two regions is half of this value. Multiplying this by the slip direction contribution across the interface (sin 15), and dividing by the grid spacing (0.5 μm), gives a slip rate gradient of 0.002026 μs^{-1}-μm^{-1}. This agrees with computed gradient in the elements below the interface to all four digits (figure 2b). The crystal lattice has distorted and rotated in the sheared elements above the interface to an orientation of 15.88°. The analytically computed slip gradient for this orientation is 0.002142 μs^{-1}-μm^{-1}. This is within 0.4 % of the numerically calculated value, which also includes effects of crystal lattice shear on the slip direction that are not included in the analytically computed gradient. A similar analysis can be performed for slip system 3, where similar accuracy is attained.

Figure 3 shows the result from a similar calculation but with the slip continuity enforced across element boundaries. The light blue element in figure 3a and the one immediately below it indicate a monotonic slip gradient for slip system 1. The gradient is quantified in figure 3b, where the colors indicate that the slip changes monotonically away from the deformation discontinuity. Slip system 3, on the other hand, shows a non-monotonic slip rate pattern near the interface (figure 3c). This is more clearly seen in figure 3d as the color changes jump to extreme values on either side of the elements at a *y*-coordinate of 2.75 μm. This lack of monotonicity is a subject for later discussion.

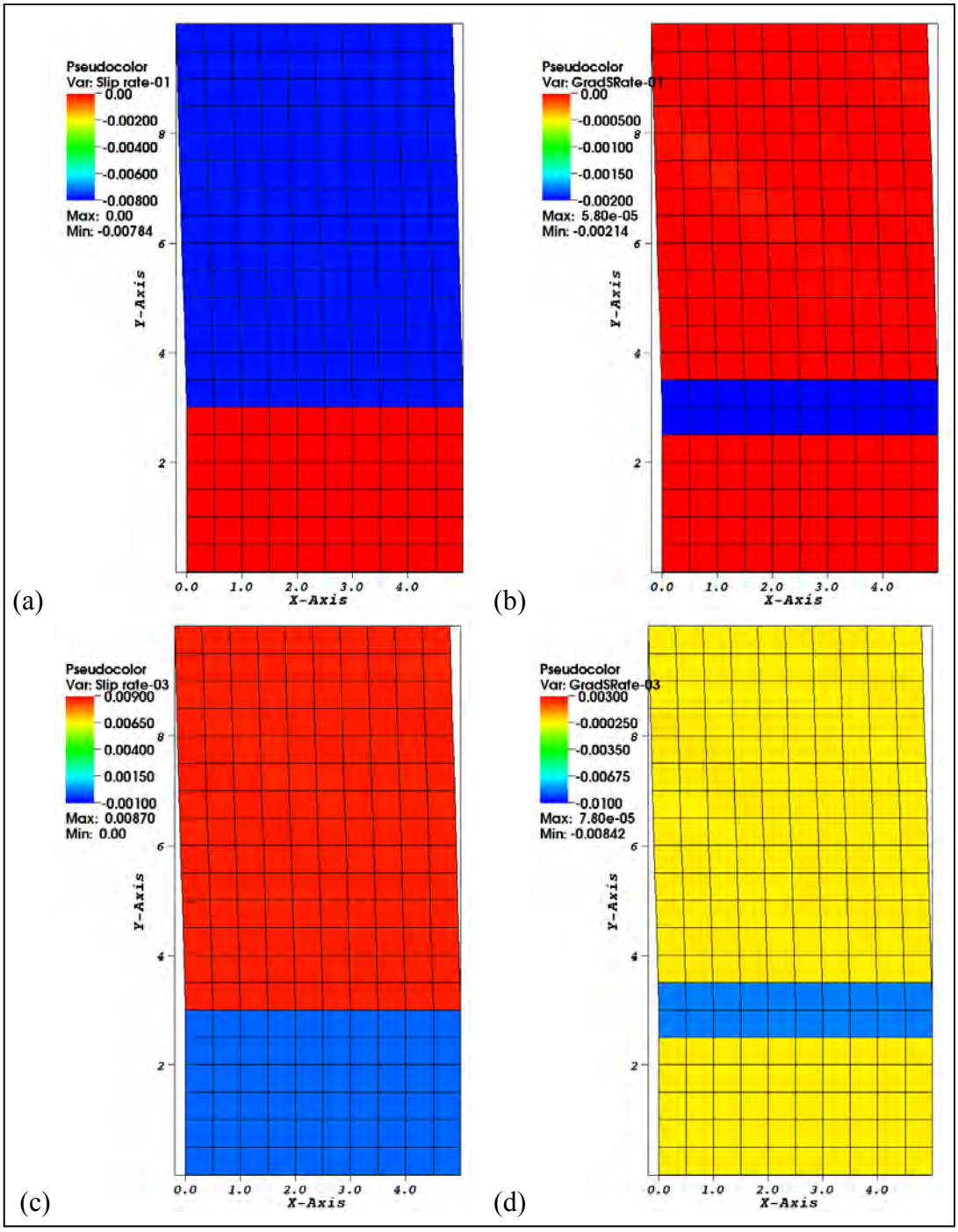

Figure 2. Simple shear of a crystal rotated 15° with the bottom 3 μm held fixed. Slip continuity is not enforced. (a) Slip rate on system 1, (b) slip gradient on system 1, (c) slip rate on system 3, and (d) slip gradient on system 3.

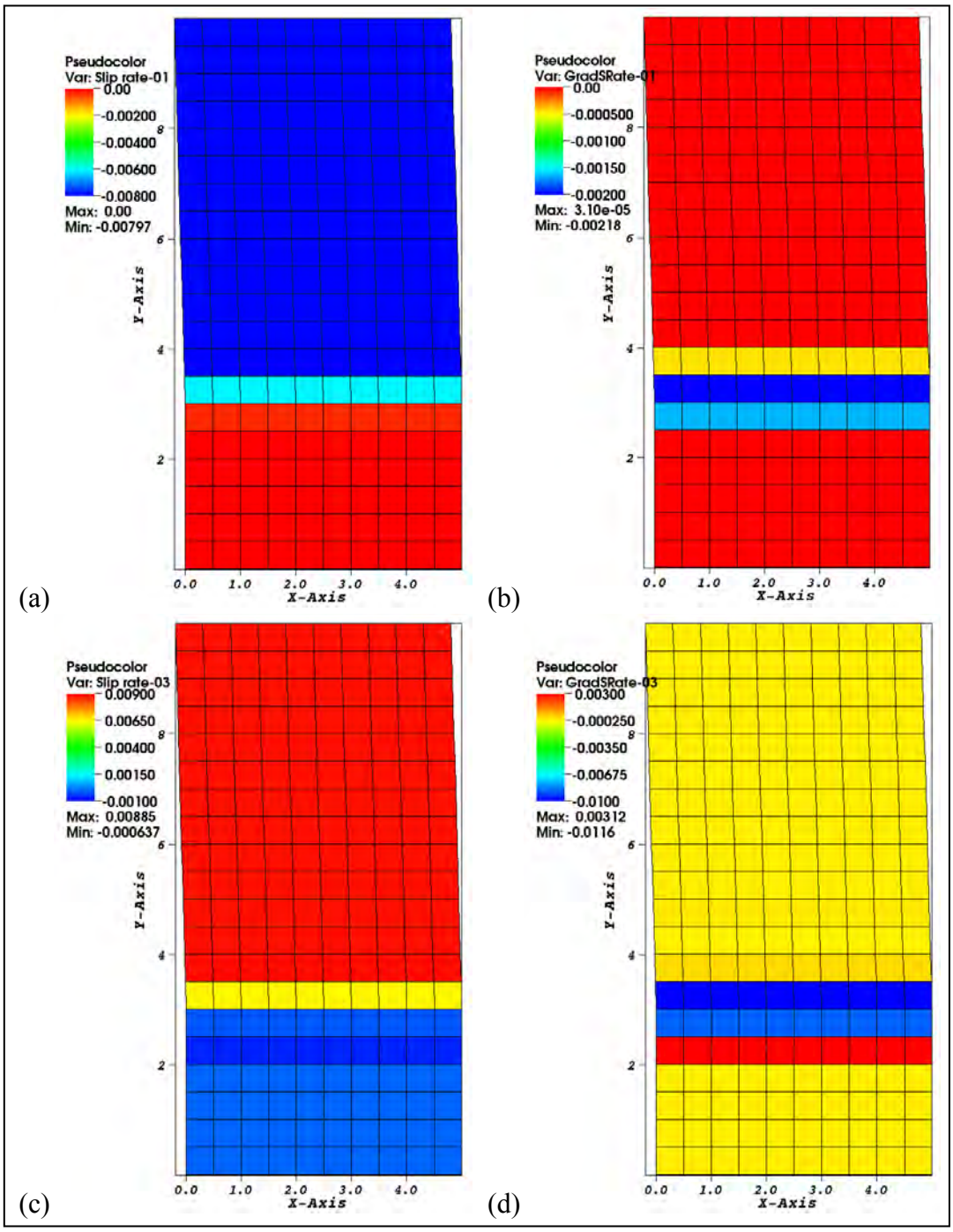

Figure 3. Simple shear of a crystal rotated 15° with the bottom 3 mm held fixed. Slip continuity is enforced. (a) Slip rate on system 1, (b) slip gradient on system 1, (c) slip rate on system 3, and (d) slip gradient on system 3.

Figure 4 shows results from a similar simple shear calculation with the crystal lattice in the reference orientation such that one of the slip directions is horizontal, parallel to the shearing direction. Here there is only slip on system 1, so only results from slip system 1 are presented. Due to the orientation of the crystal with respect to the grid, dislocations would not cross the horizontal element boundaries, and the slip continuity algorithm should not couple the deformation of neighboring elements. Figure 4a shows no indication of slip transmission, and this is confirmed by the gradient plot in figure 4b. This verifies that the simulations are only enforcing dislocation flux continuity when dislocations move across the element interfaces.

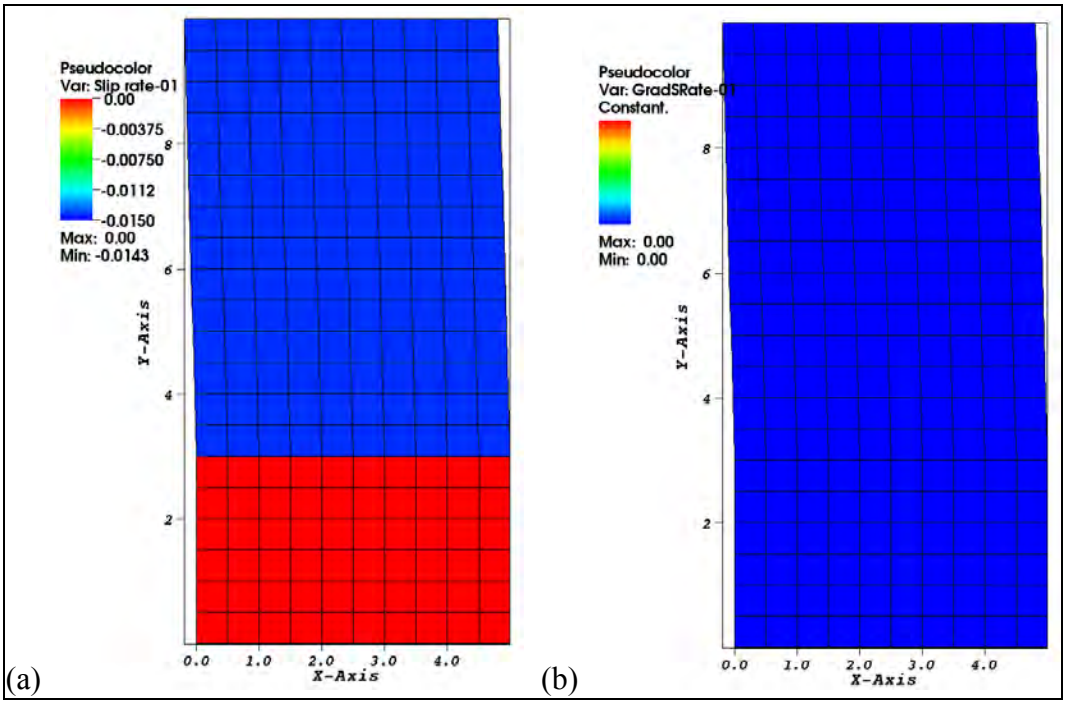

Figure 4. Simple shear of a crystal rotated 0° with the bottom 3 mm held fixed. Slip continuity is enforced. (a) Slip rate on system 1 and (b) slip gradient on system 1.

3.2 Example of Flux Continuity Effects in a Complex Deformation Field

The behavior of the numerical integration, particularly the operator split on the crystal model, was evaluated using a punch simulation where the gradients are severe. A single crystal, 40 μm wide and 20 μm high, was deformed as if indented by a flat punch over the center third of the crystal. The punch displacement rate is 10^5 μm/μs. The grid spacing for the quadrilateral mesh is 0.25 μm in both *x*- and *y*-directions. The bottom surface is prevented from vertical motion and the lateral surfaces are traction free. The initial orientation of the crystal lattice is 15° from the reference orientation so that the deformation field is asymmetric.

Plots of slip rate, on a logarithmic scale, are shown in figure 5 for the standard crystal plasticity model and the model with dislocation flux continuity enforced. As expected, enforcing dislocation flux continuity smoothes the fields along the highly strained bands and below the punch (figure 5b), but it does not appear to be excessively dispersive. It also does not appear to

diminish the peak slip rates significantly when comparing the sheared bands emanating from either side of the punch.

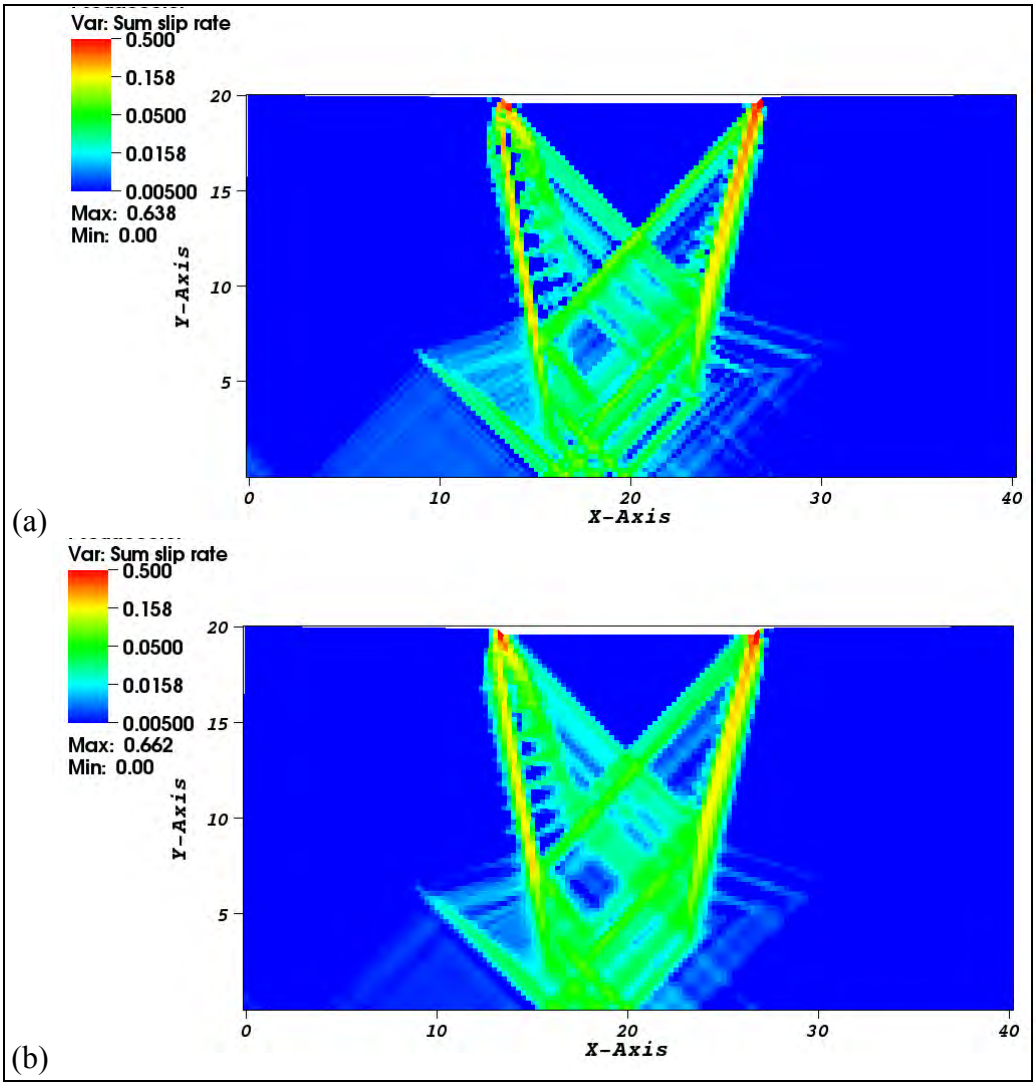

Figure 5. Slip rate contours for single crystal initially orientated 15° (a) without slip continuity enforced and (b) with slip continuity enforced.

Contours of crystal lattice rotation, with and without dislocation flux continuity enforced, are shown in figure 6. The enforcement does little to the positive lattice rotations on the left side of the punch where the rotation is focused in a narrow band. However, the peak negative rotation is significantly diminished by enforcing slip continuity, and the rotation field below the punch is also more diffuse. This is consistent with the spreading of the slip rate contours in figure 5 and is expected from the additional constraints imposed on the crystal deformation.

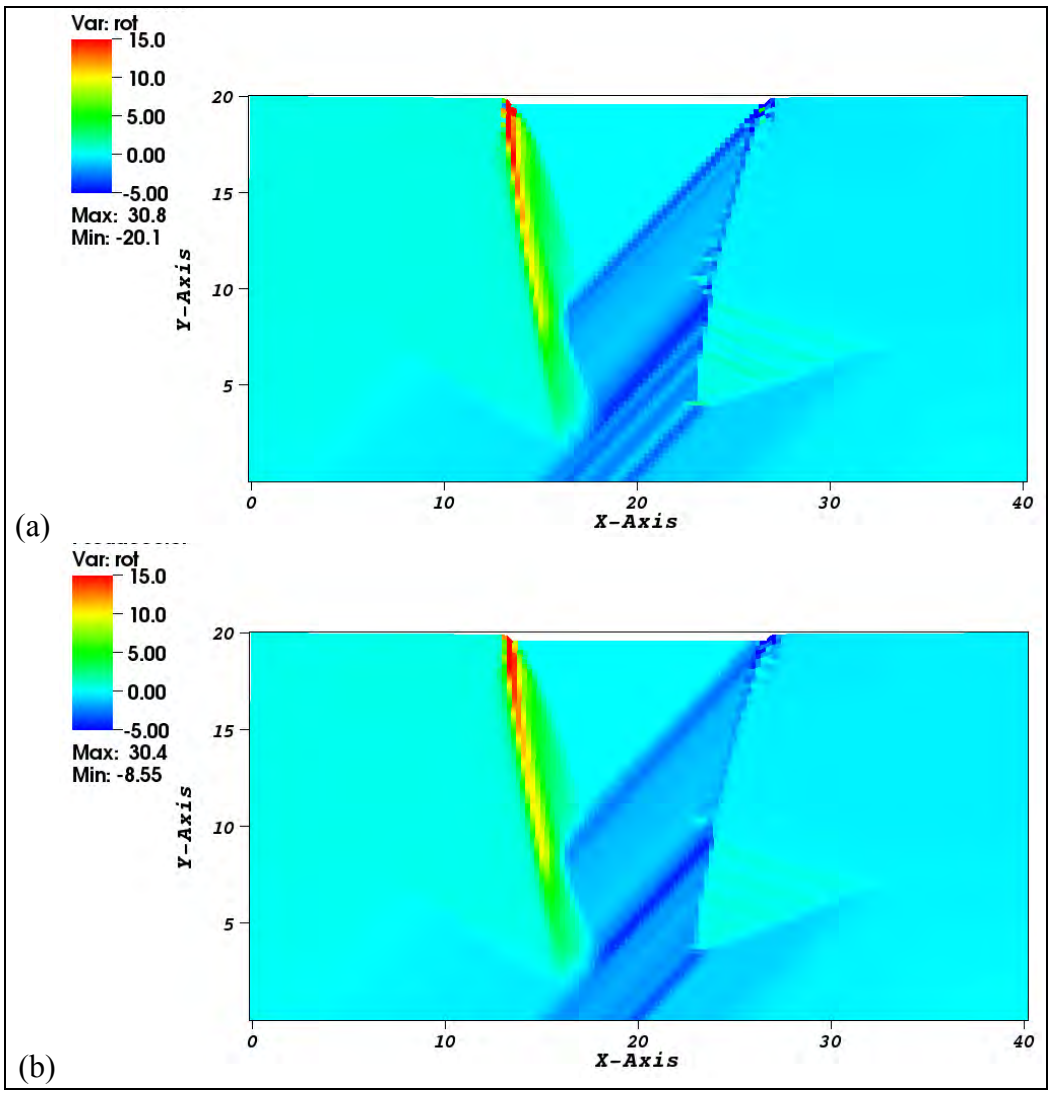

Figure 6. Crystal lattice rotation contours for single crystal initially orientated 15° (a) without slip continuity enforced and (b) with slip continuity enforced.

The punch load for the simulation with flux continuity imposed is approximately 0.5% lower than the punch load from the standard crystal plastic simulation. Since the slip system strength is prescribed to be constant in these calculations, the lower load implies that the crystal lattice is in a slightly softer orientation when dislocation flux continuity is enforced. Understanding this will require further exploration.

3.3 Exploration of Gradient Effects on Length Scale

A simple shear simulation on a thin film is run as a preliminary assessment of the effects of increasing slip resistance due to gradients in dislocation density. Strain hardening, $\beta = 0.5$, is included to smooth inhomogeneities in the deformation field triggered by noise in the explicit solution. Three sets of simulations are run: the baseline crystal plasticity model, enforcing dislocation flux continuity, and inclusion of gradient hardening in addition to enforcing

dislocation flux continuity. The lattice orientation is initially 15°, and periodic boundary conditions are applied so that only a single column of elements is needed. The film is sandwiched between, and perfectly bonded to, two stiff, horizontal dies that prohibit dislocation transmission. This creates a slip gradient that changes as the thickness of the film is varied. Simulations are run for a 10-μm-thick and a 1-μm-thick film to ascertain the size scale effect.

The slip rates are plotted in figure 7 for the 10-μm-thick film and in figure 8 for the 1-μm-thick film at a shear strain of 0.05. As expected, the standard crystal plasticity model (figures 7a and 8a) is strained uniformly through the thickness and the behavior is the same for the two film thicknesses. Since the model shears uniformly, the sides of the model are linear. With dislocation flux continuity enforced at element boundaries and zero flux enforced at the film boundaries (figures 7b and 8b), the slip is not uniform through the thickness. The slip rate in the elements near the surface is reduced due to the flux boundary condition, and the slip rate is highest in the second element from the surfaces. While there is some difference in slip rate with film thickness, it is not significant compared to the strength of the gradient near the surfaces. The sides of the model are not straight. There is a kink near the surfaces, where the slip rate is highest, and the center portion appears linear.

The addition of hardening associated with slip gradients modifies the deformation patterns in figures 7c and 8c. The total slip rate varies continuously through the thickness, and the specimen profile is sigmoidal. The slip rate is relatively uniform in the center of the 10-μm-thick film, and the gradient is concentrated at the surfaces. The gradient is spread over the entire thickness of the 1-μm-thick film. This is also reflected in the greater curvature of the thinner film.

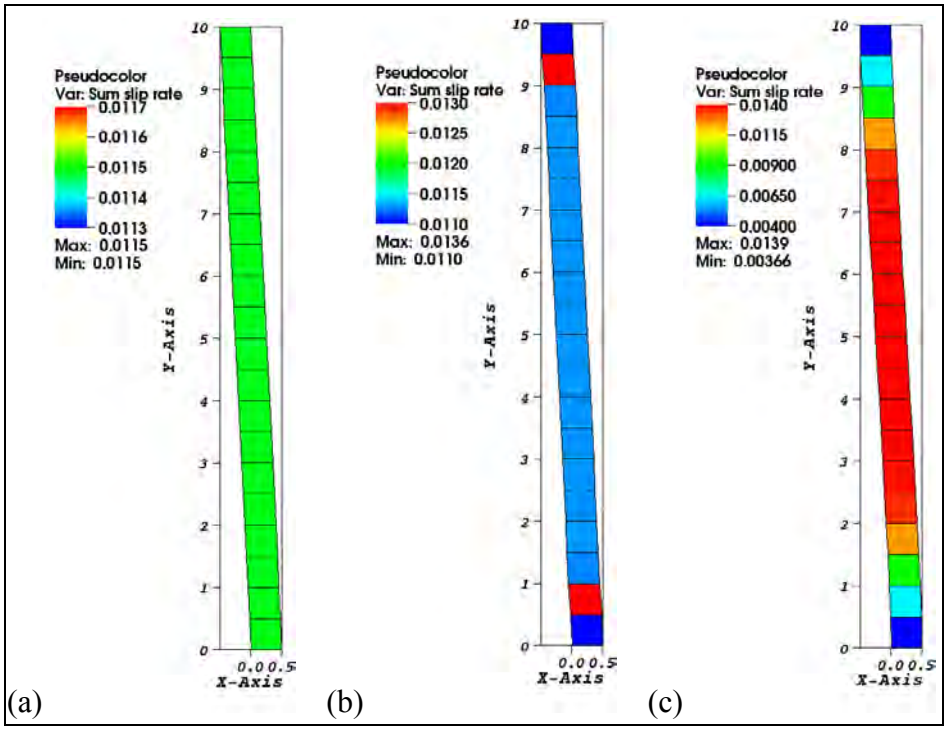

Figure 7. Slip rate sum for 10-µm-thick film simulations: (a) traditional crystal plasticity, (b) with slip continuity enforced, and (c) with slip continuity and strengthening from slip gradients.

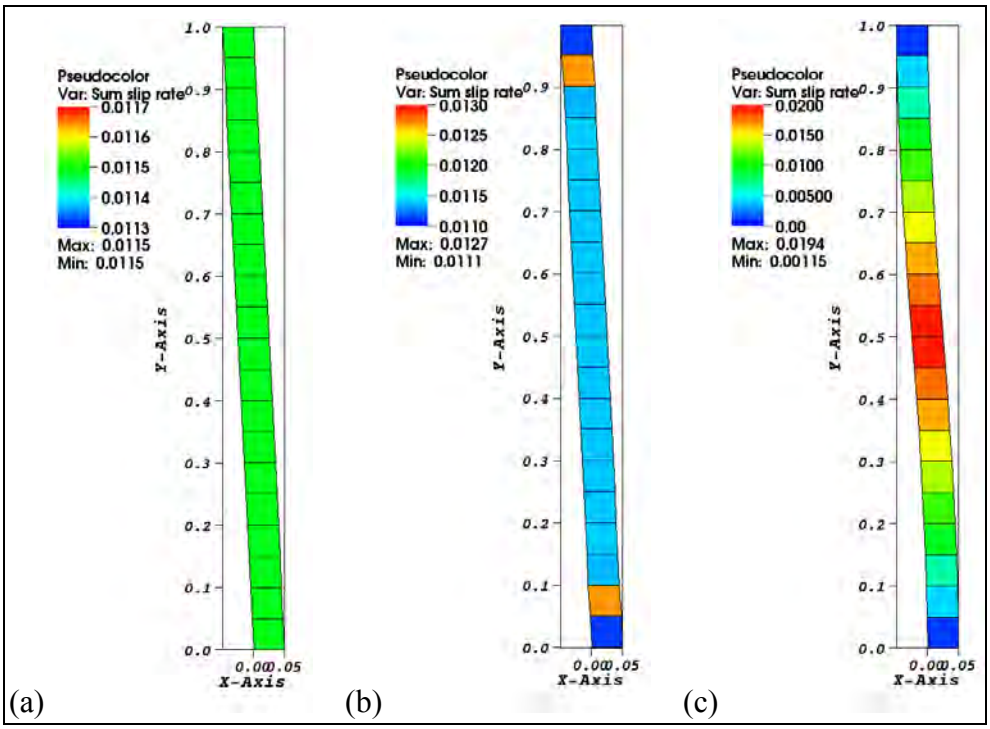

Figure 8. Slip rate sum for 1-µm-thick film simulations: (a) traditional crystal plasticity, (b) with slip continuity enforced, and (c) with slip continuity and strengthening from slip gradients.

Slip gradients, at a shear strain of 0.05, are shown in figure 9 for the 10-µm-thick film and in figure 10 for the 1-µm-thick film. Gradients are presented for slip systems 1 and 3 for the calculations with dislocation flux continuity enforced and the calculations with flux enforced plus gradient effects on hardening. The gradients from the standard crystal model are identically zero and are not shown. The gradients reflect the slip distributions given in figures 7 and 8. Just enforcing dislocation flux continuity affects only the elements near the surface, and there is no appreciable size scale effect. When the slip gradient modifies the strain hardening, the gradient on slip system 3 is significantly different for the two film thicknesses. The gradient is smooth and monotonic for the thinner film (figure 10c) but not for the thicker film (figure 9c).

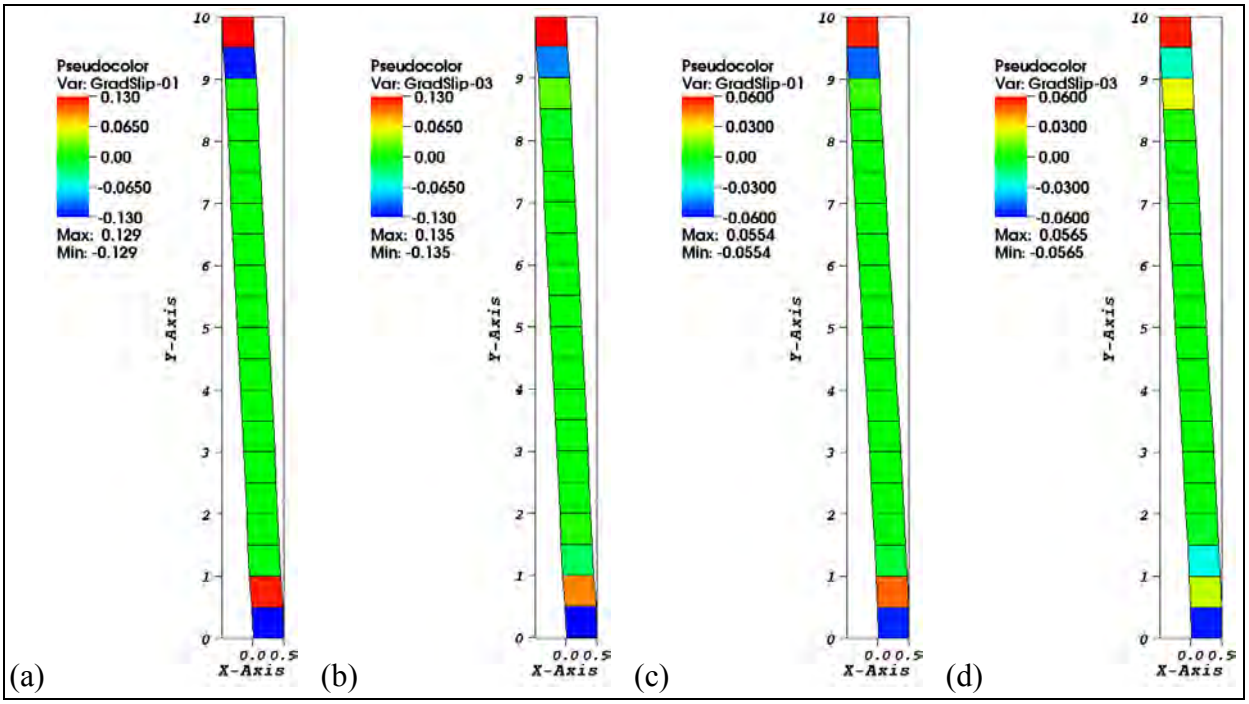

Figure 9. Slip gradient on systems 1 and 3 for 10-µm-thick film simulations: (a) and (b) with slip continuity enforced and (c) and (d) with slip continuity and strengthening from slip gradients.

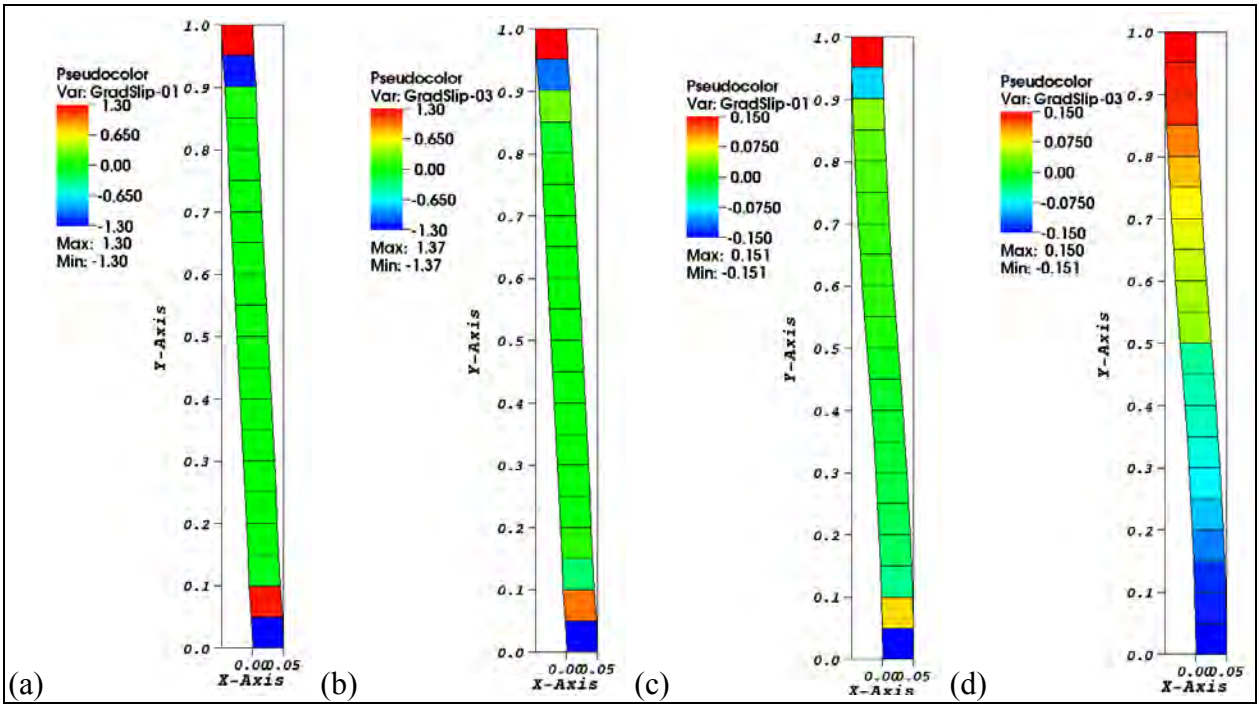

Figure 10. Slip gradient on systems 1 and 3 for 1-μm-thick film simulations: (a) and (b) with slip continuity enforced and (c) and (d) with slip continuity and strengthening from slip gradients.

The effect of dislocation flux continuity and gradient hardening is illustrated by the stress-strain curves in figure 11. The response of the standard crystal model is the same regardless of film thickness. The enforcement of dislocation flux continuity between the elements modifies the response slightly, but not enough to create a distinct line on this plot. Thus, curves from four of the six calculations appear coincident in figure 11. The effects of including gradient hardening are evident. The response of the 10-μm-thick film departs perceptibly from the baseline model, and the stress in the thinner, 1-μm-thick, film is substantially greater. It should be noted that if the crystal is initially in the reference orientation, with the crystal slip parallel to the boundaries, the dislocation flux across the horizontal element faces is zero. Consequently, there would be no flux gradient across the elements and no size effect.

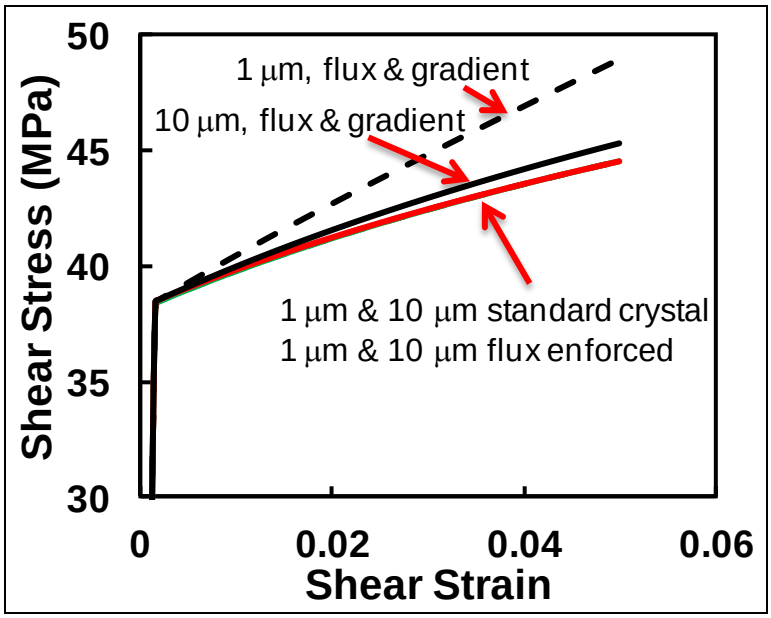

Figure 11. Stress strain curves from 1-μm-thick and 10-μm-thick films with standard crystal plasticity, with dislocation flux enforced and with flux enforced plus gradient strengthening.

4. Discussion and Future Directions

The crossed-triangle elements were implemented as a way to align element boundaries with slip planes in an effort to capture sharper gradients in the deformation field. Unfortunately, the crossed triangles still appear to give stiffer response than the constant stress quadrilaterals in most circumstances (results not shown). For large meshes using quadrilateral elements, the ratio of number of degrees of freedom to the number of incompressibility constraints enforced by the elements is 2. The crossed triangles, through a geometric serendipity (Nagtegaal et al., 1974), are not over-constrained like unstructured triangular meshes. However, the ratio of degrees of freedom to incompressibility constraints is only 4/3. Consequently, the overall response is somewhat stiffer than the quadrilaterals even though the slip aligns with element boundaries. These elements will continue to be evaluated as advancements are made to the code, since having element boundaries aligned with the slip planes could still prove useful.

Enforcing dislocation flux continuity by the operator split approach described in section 2.4 appears appropriate for smoothly varying slip fields, as in the punch problem, but the abrupt discontinuity evidenced in the simple shear examples is problematic. The oscillatory behavior has the appearance of an hourglass mode. But it could also indicate that an upwinding scheme is needed to deal with the sharp advecting gradients. The nature of the oscillatory behavior needs to be explored further before proposing a remedy. A susceptibility to hourglassing could be inherent in the chosen variable placement on the element combined with a lack of constraint on

the slip gradients at element faces. Physical stabilization of the hourglass modes would involve penalizing slip gradients from element to element by introducing additional constraints at element faces. Upwinding would involve consideration of longer-range gradients or, perhaps, borrowing ideas from the Streamline-Upwind Petrov-Galerkin methods used in finite element simulations of fluids. In either case, further development of the numerical approach will be needed. This could prove challenging.

Enforcing slip continuity does smooth the deformation field, as anticipated. However, slip continuity in the crystal plasticity model does not, by itself, appear to be sufficient to induce a proper length scale dependence in the simulations. Thus, the simple enhancement, while physically appropriate, is likely not adequate. Extending this framework to include gradient terms in the hardening relation to represent dislocation pileups and geometrically necessary dislocations does provide a length scale, consistent with results from numerous prior studies (e.g., Arsenlis et al., 2004; Gerken and Dawson, 2008; Gurtin et al., 2007; Mayeur et al., 2011). However, even with gradient hardening, the initial yield strength of the single crystal, indicated in figure 11, is unaffected. This suggests that some important physical mechanism is still missing.

The current approach is distinct from the past work in the primary variables used to calculate the gradients and the implications for boundary conditions. The proposed method uses fundamental quantities already existing in the solution, i.e., crystal slip rates, and physically intuitive boundary conditions can be applied. Other approaches introduce new degrees of freedom, such as dislocation density or geometrically necessary dislocations, which have no obvious boundary prescription. This has been an impediment to their use that could be ameliorated by the current approach.

5. References

Acharya, A. A Model of Crystal Plasticity Based on the Theory of Continuously Distributed Dislocations. *J. Mech. Phys. Solids* **2001**, *49*, 761–784.

Arsenlis, A.; Parks, D. M.; Becker, R.; Bulatov, V. On the Evolution of Crystallographic Dislocation Density in Homogeneously Deforming Crystals. *J. Mech. Phys. Solids* **2004**, *52*, 1213–1246.

Asaro, R. J. Micromechanics of Crystals and Polycrystals. *Advances in Applied Mechanics* **1983**, *21*, 1–115.

Baskaran, R.; Akarapu, S.; Mesarovic, S. D.; Zbib, H. M. Energies and Distributions of Dislocations in Stacked Pipe-ups. *Int. J. Solids, Struct.* **2010**, *47*, 1144–1153.

Becker, R. Effects of Crystal Plasticity on Materials Loaded at High Pressures and Strain Rates. *Int. J. Plast.* **2004**, *20*, 1983–2006.

Flanagan, D. P.; Belytschko, T. A Uniform Strain Hexahedron and Quadrilateral with Orthogonal Hourglass Control. *Int. J. Num. Meth. Engr.* **1981**, *17*, 679–706.

Fleck, N. A.; Hutchinson, J. W. Strain Gradient Plasticity. *Adv. Appl. Mech.* **1997**, *33*, 295–361.

Gerken, J. M.; Dawson, P. R. A Finite Element Formulation to Solve a Non-local Constitutive Model with Stresses and Strains due to Slip Gradients. *Comp. Meth. Appl. Mech. Engr.* **2008**, *197*, 1343–1361.

Gurtin, M. E.; Anand, L.; Lele, S. P. Gradient Single-crystal Plasticity with Free Energy Dependent on Dislocation Densities. *J. Mech. Phys, Solids* **2007**, *55*, 1853–1878.

Lee, T. C.; Robertson, I. M.; Birnbaum, H. K. Prediction of Slip Transfer Mechanisms Across Grain Boundaries. *Scripta Metall.* **1989**, *23*, 799–803.

Mayeur, J. R.; McDowell, D. L.; Bammann, D. J. Dislocation-based Micropolar Single Crystal Plasticity: Comparison of Multi- and Single Criterion Theories. *J. Mech. Phys. Solids* **2011**, *59*, 398–422.

Nagtegaal, J. C.; Parks, D. M.; Rice, J. R. On Numerically Accurate Finite Element Solutions in the Fully Plastic Range. *Comp. Meth. Appl. Mech. Engr.* **1974**, *4*, 153–177.

Peirce, D.; Asaro, R. J.; Needleman, A. Material Rate Dependence and Localized Deformation in Crystalline Solids. *Acta Metall.* **1983**, *31*, 1951–1976.

XDMF Web page, 18 January 2011. www.xdmf.org (accessed 2011).

6. Transitions

It is envisioned that a continuum crystal plasticity model that enforces dislocation flux continuity between adjacent elements will introduce a length scale into grain-scale continuum simulations, thereby enhancing multiscale modeling capabilities. The model could be used in grain-scale deformation simulation of metals, ceramics, and explosive materials to represent constraints of grain boundaries and surfaces more accurately. The capability aligns with crystal plasticity efforts envisioned for the Materials in Extreme Dynamics Environment Cooperative Research Alliance, anticipated to begin in fiscal year 2012 (FY12), which will serve as a venue for continued research both across the Weapons and Materials Research Directorate (WMRD) and with the Alliance.

NO. OF COPIES	ORGANIZATION
1 ELEC	ADMNSTR DEFNS TECHL INFO CTR ATTN DTIC OCP 8725 JOHN J KINGMAN RD STE 0944 FT BELVOIR VA 22060-6218
7	US ARMY RSRCH LAB ATTN RDRL WMP P BAKER ATTN RDRL-WMP C T BJERKE ATTN RDRL WMP B S BILYK ATTN RDRL WMP B J CLAYTON ATTN RDRL WMM J BEATTY ATTN RDRL CIH C J KNAP ATTN RDRL CIH C P CHUNG BLDG 390 ABERDEEN PROVING GROUND MD 21005
3	US ARMY RSRCH LAB ATTN IMNE ALC HRR MAIL & RECORDS MGMT ATTN RDRL CIO LL TECHL LIB ATTN RDRL CIO MT TECHL PUB ADELPHI MD 20783-1197